Faraday-rotation spectrum of electron spins in microcavity-embedded GaAs quantum wells

G. Salis*

IBM Research, Zurich Research Laboratory, Säumerstrasse 4, 8803 Rüschlikon, Switzerland

M. Moser

Avalon Photonics, Badenerstrasse 569, 8048 Zürich, Switzerland

Using the time-resolved magneto-optical Faraday effect, the dynamics of electron spins is measured in a GaAs quantum well embedded in a vertical one-dimensional optical cavity. The cavity leads to an enhancement of the Faraday-rotation amplitude that varies with the detuning between the QW absorption peak and the cavity resonance. We find a transition in the Faraday rotation spectrum that is triggered by the cavity detuning. This is attributed to a modification of the phase of the cavity reflectivity at the impedance-matching condition of the cavity. If the QW absorption is too small to compensate the asymmetry of the cavity mirrors, the Faraday-rotation signal is dominated by spin-induced circular birefringence, whereas contributions from circular dichroism predominate for higher quantum-well absorption. A numerical calculation of the Faraday-rotation spectrum is in good agreement with the experimental results.

PACS number(s): 78.47.+p, 78.67.−n, 78.40.−q

I. INTRODUCTION

The magneto-optic Kerr or Faraday effect allows magnetic moments to be measured on an ultrafast time scale and with high spatial resolution. Thanks to it many fruitful insights into the dynamics of magnetization in ferromagnetic metals[1] and ensembles of electron spins in semiconductor quantum structures[2] have been obtained. In the polar geometry, the polarization axis of a linearly polarized probe beam is rotated by an angle θ proportional to the magnetic moment along the beam direction. Measured angles θ are usually quite small [in bulk GaAs at room temperature they are on the order of a few μrad for an excited electron spin density of 10^{17} cm^{-2} (Ref. 3)], which makes the detection of single electron spins difficult. It has been shown that the magnitude of θ can be increased by passing the probe light multiple times through a semiconducting or magnetic sample using a one-dimensional optical cavity[4–6] or multidimensional photonic crystal structures.[7] In these measurements, a continuous-wave probe beam detects Faraday rotation (FR) originating from a Zeeman splitting of the electron levels in a static magnetic field. Recently, it was observed that also optically pumped spin polarization can be detected in a microcavity at zero pump-probe delay,[8] but no details on spin dynamics and dependence on cavity-exciton alignment were reported. Alternatively to FR, detection of polarization-resolved photoluminescence allows the study of spin dynamics, which has been extended to polaritons in the strong-coupling regime.[9–11]

Here, we demonstrate that electron-spin dynamics can be detected with enhanced FR signal in a semiconductor quantum well (QW) embedded in an asymmetric Fabry-Perot cavity. The FR signal is investigated as a function of the detuning of the cavity mode with respect to the QW absorption edge. The detuning triggers a change in the FR spectrum, which can be attributed to a threshold value for the absorption of QW electrons. If the energy of the cavity resonance is sufficiently far below the QW absorption edge, the

FR spectrum displays a single narrow peak centered at the cavity resonance. For smaller detunings, absorption increases, and a transition to a spectrum with both a positive and a negative peak within a small wavelength region is observed. The transition is attributed to a change in the reflectivity phase spectrum of the asymmetric cavity around its impedance-matching condition, combined with a crossover of birefringence-induced FR to a regime in which circular dichroism predominates. A transfer-matrix calculation of the cavity reflectivity qualitatively reproduces the observed FR spectra. An exponential time decay of the FR signal is observed across the entire resonance, with the FR amplitude changing over many orders of magnitude. Application of a transverse magnetic field allows coherent spin precession to be observed. This technique is useful to measure coherent spin dynamics of a small number of electrons at room temperature, and might provide a pathway to single-spin detection.

II. EXPERIMENTAL DETAILS

Samples are grown by metal-organic chemical vapor deposition on (001) GaAs wafers. We show data from a wafer in which three 8 nm wide GaAs/Al$_{0.18}$Ga$_{0.82}$As QWs are centered within two Bragg grating mirrors consisting of 40 (20) periods of Al$_{0.18}$Ga$_{0.82}$As/AlAs layers on the substrate (surface) side. The nominally 251 nm thick λ cavity is undoped, whereas both Bragg gratings are p-doped with a concentration of 10^{18} cm^{-3}, ensuring only small built-in electric fields across the QWs. The three QWs are separated from each other by 4 nm thick Al$_{0.18}$Ga$_{0.82}$As barrier layers. All layers are slightly wedge-shaped over the wafer area, leading to a variation of the cavity resonance wavelength between 830 and 855 nm at room temperature. Data is presented from two different samples with resonance wavelengths of 851.4 (sample 1) and 830.8 nm (sample 2) at 300 K.

Time-resolved FR is measured by dividing the beam of a mode-locked Ti:sapphire laser with a pulse length of 2–3 ps

and wavelength λ into a circularly polarized pump and a linearly polarized probe beam. The pump beam excites a spin-polarized population of electron and hole pairs in the QW. The direction of the linear polarization axis of the reflected probe beam is measured using a balanced photodiode bridge. By modulating the pump-beam intensity and using lock-in techniques, the pump-induced angular rotation θ of the linear polarization axis is resolved, with θ being proportional to the projection of spin polarization along the probe beam direction. By changing the relative delay Δt between pump and probe pulses, the dynamics of the spin polarization is traced. Previous studies in QW samples revealed that both FR (Ref. 12) and polarization-resolved photoluminescence (PL) (Ref. 13) are sensitive to the dynamics of electron rather than hole spins, and that excitonic contributions to the spin dynamics can in most cases be neglected,[14] especially at temperatures above 90 K.[15]

The two beams are focused onto a 30 μm wide spot on the sample placed in an optical cryostat. The angle of incidence is about 5° for both beams. Note that while the reflection geometry is usually referred to as Kerr rotation, we use the term FR to reflect the fact that the signal is accumulated from multiple passages of the probe light through the QWs.

III. EXPERIMENTAL RESULTS

In order to detect FR from the QW spins, the optical beams must enter the cavity, which is only possible when the photon energy matches the cavity resonance. At the same time, the photon energy should be close to the QW absorption edge, where FR is most sensitive. Both the cavity resonance and the QW absorption edge can be controlled by the temperature T.

We determine the cavity resonance from reflectivity measurements, in which a dip in the reflectivity spectrum reveals the position λ_c of the resonance. Figure 1(a) shows such a dip in reflectivity of sample 1 at 240 K. We do not observe a splitting of the reflectivity dip at any temperature, indicating that the samples are not in the strong coupling regime, in contrast to, e.g., the results presented in Ref. 8. Note that the reflectivity spectra are smeared out by the laser linewidth, which is about 0.25 nm.

The energetic position of the QW absorption edge is determined indirectly through measurements of the PL peak as detected from the side of the sample. Electron-hole pairs are excited with a continuous-wave laser tuned to 735 nm and focused to about 40 μm onto the side of the sample. The shape of the PL peak might be influenced by reabsorption at energies given by the cavity resonance. Nevertheless we assume that the observed peak positions accurately reflect the peak emission of the isolated QWs. This is because the PL spectra are much broader than the resonance linewidth [Fig. 1(b)], and no distortions in the line shape that vary with T are observed. The full width at half-maximum of the PL peaks monotonically increases with T, from 13 meV at 10 K to 45 meV at 300 K. No significant Stokes shift is expected at the elevated temperatures used in our experiement.[16,17] Therefore we may suppose that the peak absorption coincides with the peak PL.
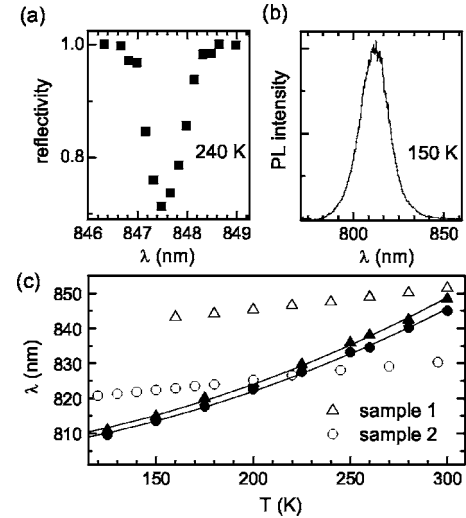

FIG. 1. (a) Reflectivity spectrum of the cavity of sample 1 at 240 K showing the cavity resonance. (b) Measured PL from the side of QW sample 1 at 150 K. (c) Wavelengths of the cavity resonance (open symbols) and of the maxima of QW PL (solid symbols) vs T for sample 1 (triangles) and sample 2 (circles).

Figure 1(c) summarizes λ_c (open symbols) and the PL peak positions (solid symbols) for the two samples as a function of T. The wavelength of the PL peak strongly increases with T because of the T-dependent band gap, whereas λ_c increases with a smaller slope of 0.06 nm/K, which is mainly attributed to a varying refractive index.[18] The different slopes of PL peak and λ_c allow its separation to be tuned by T. For the two samples, the two energies coincide at different T, which we exploit to differentiate between effects that depend on T and those that depend on the energy separation.

Time-resolved FR $\theta(\Delta t)$ is measured as a function of λ and T. The FR amplitude θ_0 is obtained by extrapolating $\theta(\Delta t)$ to $\Delta t=0$. We focus on the spectral dependence $\theta_0(\lambda)$. In Fig. 2, $\theta_0(\lambda)$ is plotted for four different T. The data is obtained on sample 1 with a pump power of 340 μW (probe power 40 μW). A transition from FR spectra with a single, positive peak below 260 K to spectra with positive and negative peaks at higher T is observed. The separation between the positive and the negative peak is very small. At 300 K the positive peak occurs at 851.3 nm and the negative peak at
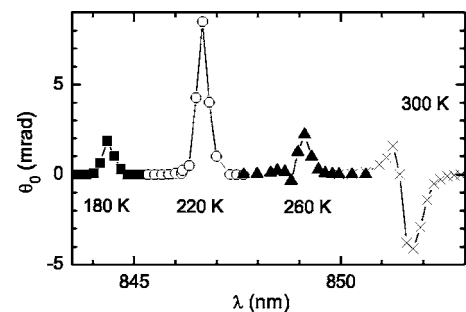

FIG. 2. FR of sample 1 at four different temperatures exhibits a transition in the FR spectra: a single positive peak for $T<260$ K and a positive and a negative peak for $T>260$ K.
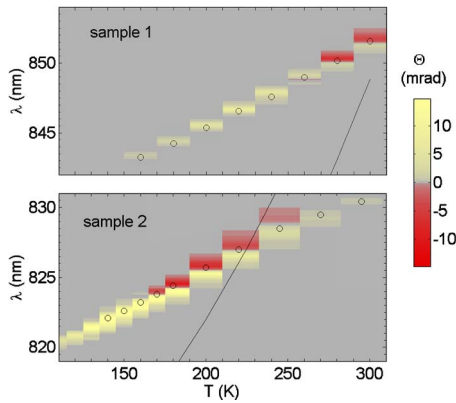
FIG. 3. (Color online) Density plot of FR vs λ and T for samples 1 and 2 show that the transition in FR spectrum occurs at different T but similar cavity-QW detuning. The solid lines indicate the position of the PL peak, the open circles represent the cavity resonance (minimum of reflectivity).

851.8 nm. In a small temperature range around the transition, θ_0 exhibits positive peaks on both sides of the negative peak.

To investigate whether the transition in the FR spectrum is related to the cavity-QW detuning or to other effects related to temperature, we measure the FR spectra on sample 2, where the cavity energy is about 37 meV smaller than that in sample 1 but the PL energies are similar [see Fig. 1(c)]. Figure 3 shows FR data from both samples encoded in a color scale and plotted vs λ and T. For sample 2 the spectral transition occurs at $T \approx 160$ K, where the cavity mode is about 15 meV below the PL peak. For comparison, the transition in sample 1 occurs 19 meV below the PL maximum. Considering the higher T and therefore larger absorption linewidth at transition for sample 1, the QW absorption at the transition is similar for the two samples. This indicates that the transition in the FR spectrum is triggered by the varying QW absorption that depends on the distance between the cavity mode and the QW absorption peak, and not by T itself. This is supported by a measurement at constant T but varying cavity mode energy (tuned by position on the sample), where a transition in the FR spectrum can also be induced (data not shown).

The FR signal decays exponentially with Δt, as shown in Fig. 4(a) for $T = 300$ K. Data is presented for three different

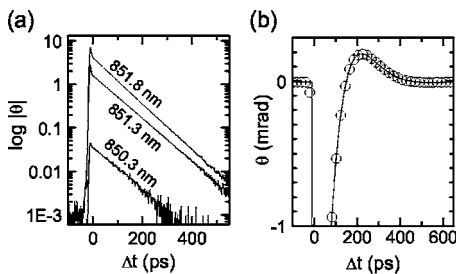
FIG. 4. (a) Time-resolved FR scans at 300 K for different λ, showing a monoexponential decay of the spin signal with a similar decay rate but different amplification across the resonance. (b) Application of a transverse magnetic field of 1.1 T leads to spin precession. Open circles are measured data at 300 K, the solid line is a fitted exponentially decaying oscillation.
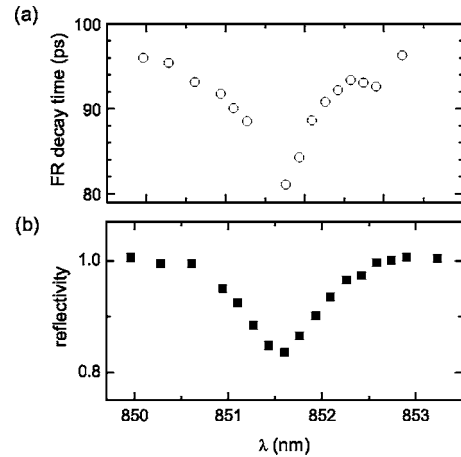

FIG. 5. (a) Measured time constant τ of the FR decay vs λ at 300 K, showing a dip at the cavity resonance. (b) Reflectivity spectrum of the cavity resonance.

wavelengths, slightly off-resonance ($\lambda = 850.3$ nm), at the positive FR peak (851.3 nm), and at the negative FR peak (851.8 nm). The decay times τ for the positive and negative peaks are 89 and 81 ps, respectively, whereas $\tau = 95$ ps at $\lambda = 850.3$ nm.

This variation in τ is further investigated by measuring a series of time-resolved FR traces across the cavity resonance. As can be seen from the results shown in Fig. 5(a), the observed sign change in θ_0 is not reflected in τ; τ displays a single dip centered close to the negative peak of θ_0 at 851.8 nm, which coincides with the minimum in cavity reflectivity [Fig. 5(b)] and therefore with the cavity resonance.

The dip in τ can be understood by the varying absorption as λ is scanned across the cavity resonance. This is evidenced by a measurement of the dependence of τ on pump power. Figure 6 shows such data obtained at 300 K and with λ at the negative FR peak. The pump power is varied from 2.5 μW to 510 μW, corresponding to excitation densities from $\approx 1 \times 10^9$ to 2×10^{11} cm^{-2} per QW and per pump pulse. As expected, the FR amplitude varies linearly with the pump power (not shown). A decrease of τ with pump power is observed, from around 100 ps below 10 μW to values of less than 80 ps above 400 μW (Fig. 6). This dependence of τ on the QW carrier excitation density is compatible with the observed dip in τ on resonance, where the QW absorption strongly increases.
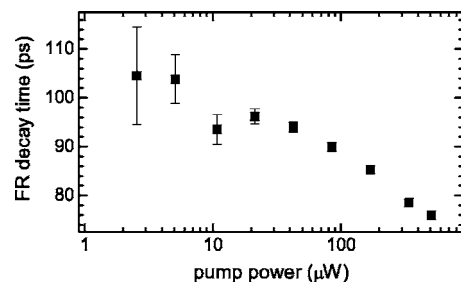

FIG. 6. The FR decay time τ shows a decrease with pump power, which explains the dip in τ at the cavity resonance. This data is obtained at 300 K and with λ tuned to the negative FR peak.

The decay time τ of the FR signal is given by both spin decay (T_s^*) and recombination of charge carriers (T_r), $1/\tau = 1/T_s^* + 1/T_r$. Time-resolved differential reflectivity measurements allow T_r to be determined.[19] From such measurements, we find T_r to decrease from around 2000 ps at 50 μW to 1430 ps at 340 μW pump power. These times are much longer than τ, therefore $\tau \approx T_s^*$ and the power dependence in T_r cannot explain the power dependence in τ. Possible explanations for a decrease in T_s^* with increasing carrier excitation density include an increase in the spin-orbit interaction due to state-filling effects and the screening of electric fields from excited electron-hole pairs.[20]

The application of a transverse field leads to coherent precession of the electron spin ensemble,[21] which allows us to measure the electron g factor. Figure 4(b) presents the spin precession measured in the cavity at $T = 300$ K and $\lambda = 851.6$ nm with a transverse magnetic field of 1.1 T. The signal can be perfectly fit with the product of an exponential decay (time constant, 85.1 ps) and a harmonic oscillation (period, 638 ps) (solid line). The oscillation period corresponds to a g-factor modulus of 0.10. This value is compatible with calculations of the electron g factor,[22] which furthermore predict a negative sign of g for the QWs used here. Similar to the observation in bulk GaAs material,[23] the g factor increases with T for the QW samples studied here (at 160 K a g-factor modulus of 0.13 is measured).

IV. DISCUSSION

In the following, the features observed in the FR spectrum are discussed. In general, FR occurs because of different optical coefficients for left- and right-circularly polarized light, which is induced by the spin polarization of the optically oriented electrons in our experiment. The FR angle θ is given by

$$\theta = \tfrac{1}{2}(\arg r_+ - \arg r_-), \tag{1}$$

where r_+ (r_-) are the complex amplitude reflectivities for right (left) circularly polarized light, which relate the amplitudes of the reflected and incoming probe beams. In order to calculate the FR spectrum, we start with the reflectivity phase spectrum of the cavity and discuss its modification due to helicity-dependent absorption and refraction in the QW. In Sec. IV A we show that an analytical expression for the amplitude reflectivity of an asymmetric Fabry-Perot cavity qualitatively explains the FR spectra measured. The subsequent section then presents the results of a more precise, numerical calculation of the cavity reflectivity, which confirm the qualitative discussion.

A. Reflectivity spectrum of an asymmetric cavity

The front and rear mirrors are described by the amplitude reflectivities $r_f(\lambda)$ and $r_r(\lambda)$, respectively. For simplicity, the wavelength dependence is omitted in the notation. The propagation of the wave amplitude between the two mirrors is given by a factor

$$p_{\pm} = e^{-\alpha_{\pm}L_{\mathrm{QW}}/2 + i\phi_{\pm}}. \tag{2}$$

Here L_{QW} is the effective width of the QW layers with absorption coefficient $\alpha_{\pm}$ and refractive index $n_{\pm}$ (the subscript $\pm$ denotes the photon helicity and accounts for circular dichroism and circular birefringence of the QWs). The phase $\phi_{\pm}$ is given by

$$\phi_{\pm} = 2\pi n_c(L - L_{\mathrm{QW}})/\lambda + 2\pi n_{\pm}L_{\mathrm{QW}}/\lambda, \tag{3}$$

where n_c is the refractive index of the cavity and L the distance between the two mirrors. For nonabsorbing Bragg mirrors, the amplitude reflectivity $r_{\pm}$ of the asymmetric Fabry-Perot cavity can be written as

$$r_{\pm} = r_f - \frac{p_{\pm}^2 r_r(1 - r_f^2)}{1 - p_{\pm}^2 r_f r_r}. \tag{4}$$

According to Eq. (1), FR occurs because of different reflectivity phases for the two photon helicities. In Eq. (4), this polarization dependence is accounted for by either helicity-dependent absorption $\alpha_{\pm}$ (circular dichroism) or the helicity-dependent refractive index $n_{\pm}$ (circular birefringence). The main reason for such effects is the unequal phase-space filling of the two spin populations,[8,24] which together with the optical selection rules leads to a different blueshift of the dielectric function for the two helicities. For a given blueshift, the resulting difference in the dielectric function is proportional to its slope, therefore FR is typically largest around absorption features of the semiconductor structure. Note that features in the real part of the dielectric function decay less rapidly with increasing distance from the peak absorption than those in the complex part do. At a sufficiently large distance, absorption can be made small while keeping the circular birefringence large enough to detect a FR signal.

In order to calculate the FR, the complex phase of $r_{\pm}$ is of interest. It exhibits a marked transition at the impedance-matching (IM) condition,[25] which is given by $r_r e^{-\alpha_{\pm}L_{\mathrm{QW}}} = r_f$. The IM defines a critical absorption $\alpha_c L_{\mathrm{QW}} \approx (r_r - r_f)/r_r$ (valid for $\alpha_c L_{\mathrm{QW}} \ll 1$). For $\alpha_{\pm} < \alpha_c$, $\arg r_{\pm}$ changes by 2π within the resonance linewidth [Fig. 7(a)]. For $\alpha_{\pm} > \alpha_c$, $\arg r_{\pm}$ displays an absorptive-type dispersion,[26] see Fig. 7(b). We will refer to the first case as "below IM," and to the second case as "above IM." The curves in Fig. 7 are calculated from Eq. (4) with $r_f = 0.9982$, $r_r = 0.9997$, $L = 244.97$ nm, $L_{\mathrm{QW}} = 24$ nm, $n_c = 3.46$, and λ-independent values for $n_{\pm}$ and $\alpha_{\pm}$. As we shall see below, the features observed in the FR spectrum can be explained by an IM transition triggered by the varying QW absorption as T is changed.

The values for r_f and r_r are obtained using a transfer-matrix approach,[27] assuming refractive indices of 3.46 and 2.98 for the 61.4 and 71.3 nm wide dielectric layers of the Bragg mirrors, respectively, and an absorption coefficient of 5 cm^{-1}. With these values, IM is expected to occur at $\alpha_c L_{\mathrm{QW}} \approx 0.0015$. If the cavity energy is sufficiently far below the QW absorption edge (low T), the cavity is below IM. As T increases, QW absorption sets in, and eventually IM is reached. At maximum absorption, the authors of Ref. 28 find $\alpha L_{\mathrm{QW}} = 0.01$ for one similar QW, which puts our cavity well above IM.
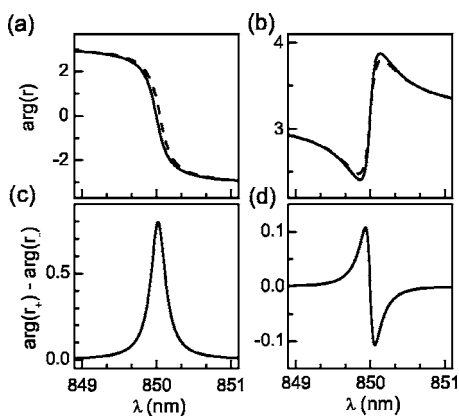
FIG. 7. Spectral phase of the reflectivity for an asymmetric Fabry-Perot cavity as obtained from Eq. (4) with parameters described in the text. In (a), the cavity is below IM, with $\alpha_\pm=0$ and $n_-=3.560$ ($n_+=3.562$) for the solid (dashed) line. In (b) the cavity is above IM, with $n_\pm=3.560$ and $\alpha_-L_{QW}=0.00240$ ($\alpha_+L_{QW}=0.00264$) for the solid (dashed) line. Differences of reflectivity phases for right- and left-circular polarization are shown in (c) below IM and in (d) above IM.

Below IM, circular dichroism has little effect on arg $r_\pm$, while circular birefringence leads to a helicity-dependent shift of the cavity resonance and therefore to a spectral displacement of arg(r_+) as compared with arg(r_-). As we will see below, $n_\pm(\lambda)$ varies slowly across the resonance. Therefore, the cavity reflectivity phase keeps the qualitative shape shown in Fig. 7(a), and FR is given by the difference between two such curves displaced in energy, leading to a single peak in $\theta(\lambda)$ [Fig. 7(c)].

Above IM, absorption significantly influences the amplitude of arg $r_\pm(\lambda)$ [Fig. 7(b)]. This gives rise to a negative and a positive peak in $\theta(\lambda)$ [Fig. 7(d)], corresponding to the observed FR spectrum above 260 K. Note that the zero crossing of $\theta_0(\lambda)$ between the positive and the negative peak follows the cavity resonance rather than the QW absorption peak. The latter would be expected from FR experiments in bare QWs without a cavity, where positive and negative peaks are centered above and below the QW absorption edge.

In this framework, the two different FR spectra measured in the experiment [Fig. 2] can thus be explained by two types of FR, having a refractive origin below IM and an absorptive one above IM. For λ close to the IM condition, a second, much smaller positive peak in $\theta(\lambda)$ emerges (see Fig. 2). This peak can be explained by a contribution of the birefringence-induced spectral shift of the reflectivity phase in a situation above IM.

For a QW without a cavity, the FR amplitude decreases monotonically with T. Typical values are well below 1 mrad for GaAs QWs in the temperature range between 100 and 300 K and a pump power of 1 mW. In contrast, the complex T dependence shown in Fig. 3 clearly demonstrates the cavity-related signal enhancement. Largest signals are expected and measured just below IM, where the phase of the reflected light changes by 2π within a small region on the order of the resonance linewidth [Fig. 7(a)], and thus a small helicity-dependent spectral shift of the reflection phase leads
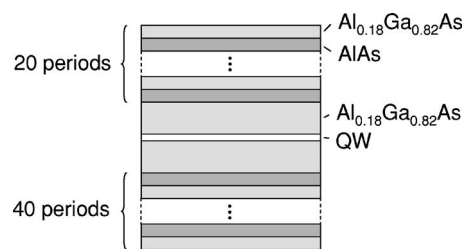

FIG. 8. Layer sequence of the calculated structure. A single $Al_{0.18}Ga_{0.82}As$ (AlAs) layer of the Bragg mirror is 61.4 nm (71.3 nm) thick. Two spacer layers, each 110.3 nm thick, and a 24 nm wide QW layer form the λ cavity.

to a large FR signal enhancement (proportional to the cavity Q-factor[29]). At energies farther below the QW absorption edge (lower T), the slope of the dispersion decreases, leading to smaller FR signals because of a smaller spin-induced circular birefringence. Similarly, for higher T, absorption increases and thus the modulation of the reflectivity phase on resonance decreases, which together with a decreasing dispersion slope leads to smaller FR amplitudes. Moreover, the increase in QW absorption raises the cavity Q-factor, which reduces the FR enhancement even more.

B. Transfer-matrix calculation of Faraday rotation spectrum

By numerically calculating the cavity FR using a transfer-matrix approach, we provide further support of the conclusions above, which are based on several assumptions. For instance, it was assumed that $n_\pm$ and $\alpha_\pm$ are constant across the resonance. Furthermore, Eq. (4) is only valid for nonabsorbing mirrors, whereas an absorption coefficient of ~ 5 cm^{-1} in the p-doped layers of the Bragg mirrors is expected, as extrapolated from free-carrier absorption.[30,31] In addition, a wavelength dependence of the mirror reflectivity phase is known to significantly decrease the width of the cavity resonance peak.[32] A numerical calculation of the cavity reflectivity takes these factors into account.

In the calculation, the entire stack of dielectric layers (Fig. 8) is considered, including the two Bragg mirrors. Accordingly, the thicknesses, refractive indices and absorption coefficients of the individual layers must be known. A constant refractive index of 3.46 for $Al_{0.18}Ga_{0.82}As$ and of 2.98 for AlAs is assumed. The absorption of the Bragg mirrors is set to 5 cm^{-1}. The absorption spectrum of the QW is inferred from PL measurements and literature data, and the QW refractive index spectrum is then calculated using the Kramers-Kronig relation.

The absorption spectrum is modelled with a peak absorption of 0.006 for the three QWs and a full-width at half-maximum of 40 meV, dropping to a plateau at 80% on the high-energy side, see Fig. 9(a). We assume the absorption peak to have Gaussian shape on the low-energy side with the same linewidth as the measured PL peak. The peak absorption is extrapolated from published data on high-quality $Al_{0.3}Ga_{0.7}As/GaAs$ QWs,[28] where an absorption spectrum with a peak of 0.01 per QW and a full-width at half-maximum of ≈ 8 meV is found. This linewidth is about five times smaller than our PL linewidth. Assuming similar oscil-
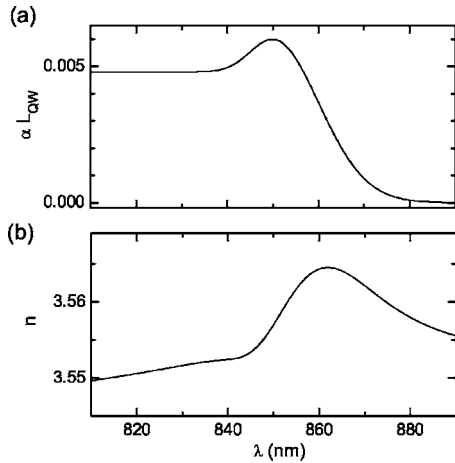
(a)

(b)

FIG. 9. (a) Absorption spectrum for the three QWs used for the transfer-matrix calculation. (b) Refractive index as obtained from (a) with the Kramers-Kronig relation and by adding a constant offset of 2.55.

lator strengths, the peak absorption will then be about five times smaller in our samples, which leads to the peak absorption of 0.006 for three QWs. The samples described in Ref. 28 display a pronounced excitonic character, with the absorption decaying to a level of about 50% on the high-energy side of the peak. Because of the smaller quantum confinement, the relatively thin barrier between the three QWs, the probably stronger layer-thickness fluctuations and the larger number of defects related to the different growth technique used, we anticipate small excitonic features in our samples, i.e., only a weakly pronounced peak in absorption, which we take into account by assuming a plateau at 80% on the high-energy side of the absorption peak.

Using the Kramers-Kronig relation, the refractive index of the well is numerically calculated from the absorption spectrum, as shown in Fig. 9(b). A constant offset has been added to bring the refractive index close to the value of bulk GaAs of 3.56. The spin-induced circular birefringence and dichroism are modelled as a spectral shift of the absorption and the refractive index by ∓ 0.1 meV, where the sign is given by the photon helicity. By calculating $r_{\pm}$ with a transfer-matrix approach[27] and using Eq. (1), we obtain the FR spectra of the cavity-QW system. Figure 10 shows five calculated spectra obtained for different energy detunings between the absorption peak and the cavity resonance. For a detuning of more than 31 meV, the cavity is below IM, and a single positive peak in FR is obtained. Around 31 meV, a transition to a double-peaked spectrum occurs. The shape of the spectra is similar to the experimental results. As in sample 1 at 260 K, the calculated curve displays two positive and a negative peak at transition; however, the peaks are weighted differently. This discrepancy might be related to helicity-dependent saturation effects[8] that contribute to FR in addition to the blueshift of the dielectric function.

We do not expect to reproduce the FR spectra quantitatively with the calculation. For instance, the calculated energy difference of 31 meV between the absorption peak and the cavity mode at IM is larger than the experimentally observed one of 19 meV. As this value is given by the absorp-
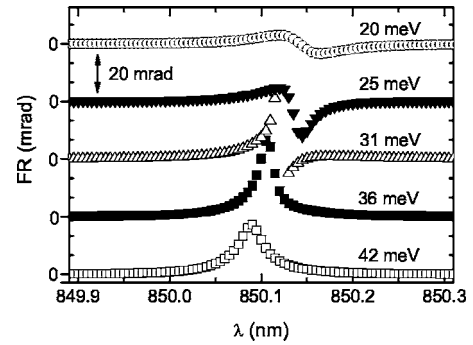

FIG. 10. Numerical calculation of the cavity-QW FR spectrum for five different cavity detunings. Results are obtained with an assumed helicity-dependent blueshift of ±0.1 meV for the QW dispersion. At a detuning of 31 meV, a crossing of the cavity IM leads to a transition of the FR spectrum as observed in the measurement.

tion value at IM, it strongly depends on the peak value and the linewidth of the QW absorption as well as on the cavity mirror reflectivities. All these quantities were not measured and thus can only be estimated here. For instance, fluctuations in the mirror layer thickness might lead to a reduction of the mirror reflectivities and therefore to a change of the IM condition, as well as to a broadening of the resonance linewidth and therefore to a decrease of the FR enhancement. Still, the calculation clearly reproduces the observed transition in FR spectrum as well as the evolution of relative peak heights as a function of cavity detuning.

Because of the finite laser linewidth of about 0.25 nm, narrow spectral features in $\theta(\lambda)$ are smeared out. Especially above IM, where the positive and the negative peak are close to each other, this might lead to a decrease of the measured FR amplitudes. Moreover, as the wavelength of the pump beam follows the probe beam, a varying number of charge carriers is excited as the probe wavelength is scanned, as can be seen by the dip in spin lifetime across the resonance [Fig. 3]. As θ_0 is proportional to the number of excited electron spins, this leads to a narrowing of the FR spectra, but does not change the observed sign changes in the FR.

V. CONCLUSIONS

In conclusion, enhancement of time-resolved FR in an asymmetric cavity is demonstrated. Two different regimes are accessed for low and high QW absorption, corresponding to a cavity below and above impedance matching. In contrast to FR without a cavity, the FR signal in a cavity above IM also depends on spin-induced circular dichroism, and not only on circular birefringence. The enhancement of the FR at wavelengths away from the semiconductor absorption peak is of interest for single-spin detection in semiconductor quantum structures, especially if the absorption of photons should be minimized as is required, e.g., in the readout of quantum information.[29] In addition, this work suggests that the technique of FR is a sensitive tool to investigate phase spectra of cavity-reflection and transmission coefficients.

*Electronic address: gsa@zurich.ibm.com

[1] Y. Acremann, C. Back, M. Buess, O. Portmann, A. Vaterlaus, D. Pescia, and H. Melchior, Science **290**, 492 (2000).

[2] D. D. Awschalom and J. M. Kikkawa, Phys. Today **52**, 33 (1999).

[3] A. V. Kimel, F. Bentivegna, V. N. Gridnev, V. V. Pavlov, R. V. Pisarev, and T. Rasing, Phys. Rev. B **63**, 235201 (2001).

[4] A. V. Kavokin, M. R. Vladimirova, M. A. Kaliteevski, O. Lyngnes, J. D. Berger, H. M. Gibbs, and G. Khitrova, Phys. Rev. B **56**, 1087 (1997).

[5] E. Takeda, N. Todoroki, Y. Kitamoto, M. Abe, M. Inoue, T. Fujii, and K. Arai, J. Appl. Phys. **87**, 6782 (2000).

[6] C. Gourdon, V. Jeudy, M. Menant, D. Roditchev, L. A. Tu, E. L. Ivchenko, and G. Karczewski, Appl. Phys. Lett. **82**, 230 (2003).

[7] C. Koerdt, G. L. J. A. Rikken, and E. P. Petrov, Appl. Phys. Lett. **82**, 1538 (2003).

[8] D. Pereda Cubian, M. Haddad, R. André, R. Frey, G. Roosen, J. L. Arce Diego, and C. Flytzanis, Phys. Rev. B **67**, 045308 (2003).

[9] M. D. Martín, G. Aichmayr, L. Viña, and R. André, Phys. Rev. Lett. **89**, 077402 (2002).

[10] P. G. Lagoudakis, P. G. Savvidis, J. J. Baumberg, D. M. Whittaker, P. R. Eastham, M. S. Skolnick, and J. S. Roberts, Phys. Rev. B **65**, 161310(R) (2002).

[11] I. A. Shelykh, K. V. Kavokin, A. V. Kavokin, G. Malpuech, P. Bigenwald, H. Deng, G. Weihs, and Y. Yamamoto, Phys. Rev. B **70**, 035320 (2004).

[12] M. Poggio, G. M. Steeves, R. C. Myers, N. P. Stern, A. C. Gossard, and D. D. Awschalom, Phys. Rev. B **70**, 121305(R) (2004).

[13] A. P. Heberle, W. W. Rühle, and K. Ploog, Phys. Rev. Lett. **72**, 3887 (1994).

[14] T. Amand, X. Marie, P. L. Jeune, M. Brousseau, D. Robart, J. Barrau, and R. Planel, Phys. Rev. Lett. **78**, 1355 (1997).

[15] A. Malinowski, R. S. Britton, T. Grevatt, R. T. Harley, D. A. Ritchie, and M. Y. Simmons, Phys. Rev. B **62**, 13034 (2000).

[16] M. Gurioli, A. Vinattieri, J. Martinez-Pastor, and M. Colocci, Phys. Rev. B **50**, 11817 (1994).

[17] J. Humlíček, E. Schmidt, L. Bočánek, R. Švehla, and K. Ploog, Phys. Rev. B **48**, 5241 (1993).

[18] B. Tell, K. F. Brown-Goebeler, R. E. Leibenguth, and F. M. Baez, Appl. Phys. Lett. **60**, 683 (1991).

[19] F. Fernández-Alonso, M. Righini, A. Franco, and S. Selci, Phys. Rev. B **67**, 165328 (2003).

[20] I. Žutić, J. Fabian, and S. D. Sarma, Rev. Mod. Phys. **76**, 323 (2004).

[21] J. J. Baumberg, D. D. Awschalom, N. Samarth, H. Luo, and J. K. Furdyna, Phys. Rev. Lett. **72**, 717 (1991).

[22] E. L. Ivchenko and A. A. Kiselev, Sov. Phys. Semicond. **26**, 827 (1992).

[23] M. Oestreich and W. W. Rühle, Phys. Rev. Lett. **74**, 2315 (1995).

[24] M. J. Snelling, P. Perozzo, D. C. Hutchings, I. Galbraith, and A. Miller, Phys. Rev. B **49**, 17160 (1994).

[25] B. Pezeshki, G. A. Williams, and J. J. S. Harris, Appl. Phys. Lett. **60**, 1061 (1991).

[26] Y. V. Troitskii and B. I. Troshin, Opt. Spectrosc. **87**, 133 (1999).

[27] P. Yeh, *Optical Waves in Layered Media* (Wiley, New York, 1988).

[28] D. A. B. Miller, D. S. Chemla, D. J. Eilenberger, P. W. Smith, A. C. Gossard, and W. T. Tsang, Appl. Phys. Lett. **41**, 679 (1982).

[29] M. Sugita, S. Machida, and Y. Yamamoto, quant-ph/0301064 (unpublished).

[30] H. Y. Fan, "Effects of free carriers on the optical properties," *Optical Properties on III-V Compounds. Semiconductors and Semimetals* (Academic, New York, 1967), Vol. 3.

[31] D. I. Babic, Ph.D. dissertation, University of California, Santa Barbara (unpublished).

[32] R. P. Stanley, R. Houdré, U. Oesterle, M. Gailhanou, and M. Ilegems, Appl. Phys. Lett. **65**, 1883 (1994).